Available online at www.sciencedirect.com
SCIENCE DIRECT
Journal of Solid State Chemistry 179 (2006) 2554–2561
JOURNAL OF SOLID STATE CHEMISTRY
www.elsevier.com/locate/jssc

# Electrochemical reaction of lithium with nanosized vanadium antimonate

Julián Morales[a], Luis Sánchez[a,*], Francisco Martín[b], Frank Berry[c]

[a]Departamento de Química Inorgánica e Ingeniería Química, Facultad de Ciencias, Campus de Rabanales, Edificio Marie Curie, Universidad de Córdoba, 14071 Córdoba, Spain
[b]Laboratorio de Materiales y Superficie (Unidad Asociada al CSIC), Universidad de Málaga, Spain
[c]Department of Chemistry, The Open University, Walton Hall, Milton Keynes MK7 6AA, UK

Received 17 January 2006; received in revised form 21 April 2006; accepted 7 May 2006
Available online 13 May 2006

**Abstract**

Nanometric vanadium antimonate, $VSbO_4$, was prepared by mechanical milling from $Sb_2O_3$ and $V_2O_5$ and characterized by X-ray diffraction (XRD), transmission electron microscopy (TEM), Mossbaüer spectroscopy (MS) and X-ray photoelectron spectroscopy (XPS) techniques. Its reactivity towards lithium was examined by testing $Li/VSbO_4$ cells under galvanostatic and potentiostatic regimes. The amount of Li inserted was found to be consistent with a two-step process involving the reactions (i) $VSbO_4 + 8\ Li \rightarrow Sb + V + 4\ Li_2O$ and (ii) $Sb + 3\ Li \rightarrow Li_3Sb$, the former being virtually irreversible and the latter reversible as suggested by the shape of the anodic and cathodic curves. Ex situ XPS measurements of the discharged and charged electrode provided direct evidence of the formation of alloyed Sb and confirmed the results of the potentiostatic curves regarding the irreversible or reversible character of the previous reactions. The $Li/VSbO_4$ cell exhibited acceptable electrochemical performance, which surpassed that of other Sb-based compounds as the likely result of the formation of V and its associated enhanced electrode conductivity.


*Keywords:* Vanadium antimonate; Electrode; Lithium batteries

## 1. Introduction

Although carbon-based materials are the most common choice for anodes in commercial lithium (Li)-ion batteries at present, there is an ongoing search for alternative materials to replace them. In the last decade, such a search has focussed primarily on systems such as Li-alloys and transition metal compounds (oxides, phosphides and nitrides). Li-alloys have attracted much attention by virtue of their high capacity and low reactive potentials [1]. The high theoretical capacity of antimony (Sb) upon reaction with Li (660 A h/kg) has proposed comprehensive studies of some Sb-based intermetallic compounds (viz $MSb_x$ with $1 < x < 3$ and $M =$ Ti, Mn, Fe, Co, Ni, Cu, Zn, In, Sn [2–11] as potential anode materials for Li-ion batteries. These alloys exhibit an improved cycling behavior relative to pure Sb. The transition metal, which acts as inert matrix in the electrochemical process, accommodates the volumes changes in $Li_xSb$ active species during the lithiation and delithiation processes. However, cycling results in pulverization of active particles and hence in rapid capacity fading by effect of the drastic volume changes undergone by these intermetallic systems. This results in inadequate long-term cycling capabilities and rules out practical application.

There have been several attempts at alleviating the mechanical stress. Thus, reversibility in these intermetallic electrodes can be markedly improved by using (i) selected compounds with special structures such as $Cu_2Sb$ [12] or $Mn_2Sb$ [3], and (ii) thin-films [13] or nanosized materials [7,14]. In the former case, the lithiated product ($Li_2Cu_2Sb$) bears a strong structural relationship with its parent compound ($Cu_2Sb$). In the latter, the diffusion path for Li-ions and volume changes in active particles are reduced.

*Corresponding author. Tel.: +34 957 218620; fax: +34 957 218621.
*E-mail address:* luis-sanchez@uco.es (L. Sánchez).

0022-4596/$ - see front matter © 2006 Elsevier Inc. All rights reserved.
doi:10.1016/j.jssc.2006.05.003

Sb-based oxides have been underexplored as an alternative to improving the electrochemical performance of Sb. Tin compounds (SnO [15], $SnO_2$ [16], $CaSnO_3$ [17]) have proved especially efficient, even though they exhibit largely irreversible capacity during the first charge–discharge process. Li et al. [18] were the first to study the electrochemical reaction of $Sb_2O_3$ with Li. The poor reversibility found was subsequently mitigated by using Sb-based oxides as thin films electrodes [19]. Recently, we found a cell made from $SbPO_4$ to perform acceptably [20]. Although $Li_3PO_4$ is a poorly conductive matrix, it exhibits good cycling properties. This paper reports the electrochemical properties of nanometric vanadium antimonite ($VSbO_4$) in Li cells. The compound was obtained in the form of nanosized particles by prolonged grinding, and was characterized by X-ray diffraction, Mossbaüer spectroscopy (MS) and X-ray photoelectron spectroscopy (XPS). Also, its reactivity towards Li was examined in Li cells of the types Li/EC–DEC 1 M $LiPF_6$/$VSbO_4$ under both potentiostatic and galvanostatic regimes.

## 2. Experimental

$VSbO_4$ was prepared from stoichiometric mixtures of commercial grade $V_2O_5$ and $Sb_2O_3$. The mixtures were dry milled in the air in a Restch PM400 planetary ball mill, using stainless steel vials (250 mL) and balls (20 mm) at 200 rpm for 70 h. The powder to ball weight ratio was 1:20.

X-ray powder diffraction (XRD) patterns were recorded on a Siemens D5000 X-ray diffractometer, using Cu $K\alpha$ radiation and a graphite monochromator, in steps of 0.02° and 0.6 s. Transmission electron microscopy (TEM) images were obtained with a JEOL 2000fx microscope.

The $^{121}$Sb Mossbaüer spectrum was recorded from powdered samples, using a constant acceleration spectrometer and a $Ca^{121}SbO_3$ source at 77 K. X-ray photoelectron spectra were recorded on a Physical Electronics PHI 5700 spectrometer, using non-monochromated Mg$K\alpha$ radiation ($h\nu = 1253.6$ eV) and a hemispherical analyzer operating at a constant pass energy of 29.35 eV. Spectra were recorded with the X-ray generator operating at 15 kV and 20 mA. The energy scale of the spectrometer was calibrated by using the Cu 2$p$3/2, Ag 3$d$5/2 and Au 4$f$7/2 photoelectron lines at 932.7, 368.3 and 84.0 eV, respectively. The vacuum in the analysis chamber was better than $10^{-9}$ Torr. Binding energies were corrected against that for C 1$s$ of adventitious carbon (and the methyl group) fixed at 284.8 eV together with the F 1$s$ at 685.5 eV. Samples were mounted on a holder without adhesive tape and kept under high vacuum in the preparation chamber overnight prior to transfer to the analysis chamber of the spectrometer. Survey spectra over the range 0–1100 eV were recorded at a 187.85 pass energy, each region being scanned several times to ensure an adequate signal-to-noise ratio. A $4 \times 4$ mm sample area was sputtered with 4 keV $Ar^+$; the sputter rate was assumed to be $\sim$2.1 nm min$^{-1}$ as determined for $Ta_2O_5$ under identical sputtering conditions. Spectra were processed by using PHI-Access V.6 and Multipak software, both from Physical Electronics. High-resolution spectra were fitted after Shirley background correction. Satellite subtraction was carried out for the V 2$p$ region before fitting. Surface atomic concentrations were determined from peak areas, using Shirley background subtraction and sensitivity factors provided by the spectrometer manufacturer (Physical Electronics, Eden Prairie, MN). In order to avoid reduction of higher metallic oxidation states by X-rays, spectra were collected with short acquisition times. Ex situ XPS measurements were performed on the acetonitrile-washed pellet from the dismantled cell. All manipulations were done under an argon atmosphere; also, a special glove-box connected to the spectrometer antechamber allowed samples to be transferred to the spectrometer without direct contact with air.

Electrochemical measurements were performed in two electrode cells, using Li as a counter-electrode. The electrolyte was Merck battery electrolyte LP 40 (EC:DEC = 1:1 w/w, 1 M $LiPF_6$). Electrode pellets were prepared by pressing, in an stainless-steel grid, ca. 4 mg of active material with polytetrafluoroethylene (PTFE) (5 wt%) and acetylene black (10 wt%) at 4 ton. Galvanostatic tests were conducted at a rate of $C/12$ ($C$ being defined as 1 $Li^+$ ion exchanged in 1 h). Step potential curves were recorded at 2.5 mV/0.22 h per step. All electrochemical measurements were controlled via a MacPile II potentiostat–galvanostat.

## 3. Results and discussion

Fig. 1 shows the X-ray powder diffraction pattern for the $VSbO_4$ sample. The characteristic peaks of vanadium antimonate [21] were observed after 70 h of milling and the crystallite size as determined using the Scherrer equation [22] was ca. 23 nm. The TEM image (Fig. 2) showed agglomerates of rounded nanoparticles, ca. 25 nm

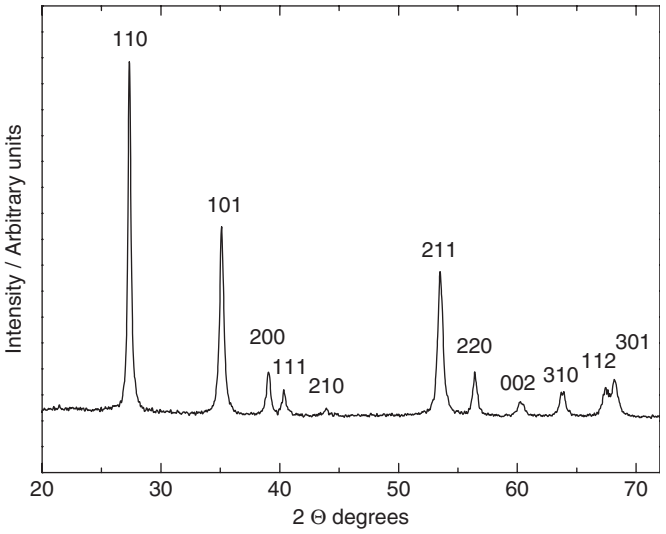


Fig. 1. XRD pattern for the $VSbO_4$ sample.

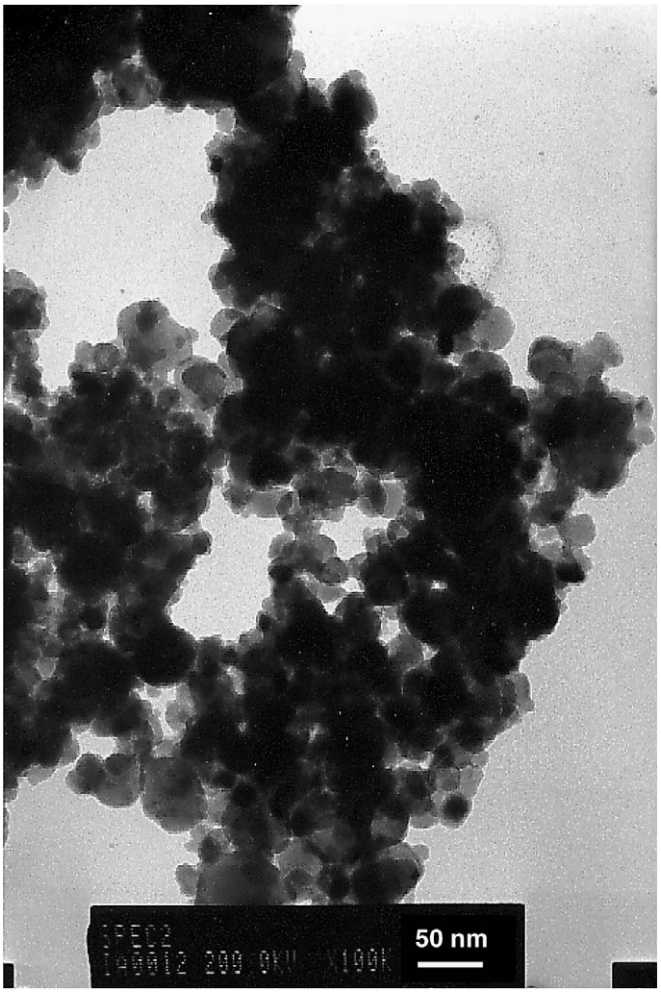


Fig. 2. TEM image of the $VSbO_4$ sample.

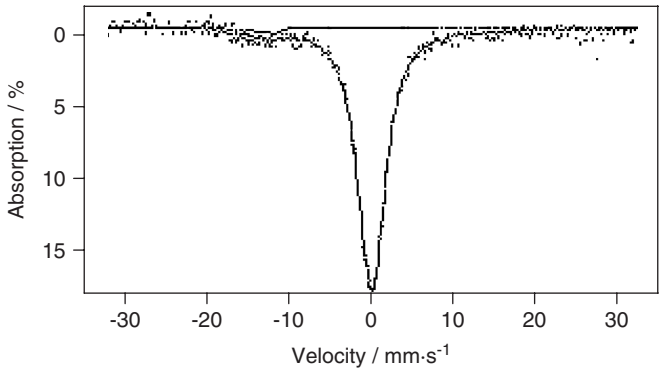


Fig. 3. $^{121}Sb$ Mössbauer spectrum for the $VSbO_4$ sample.

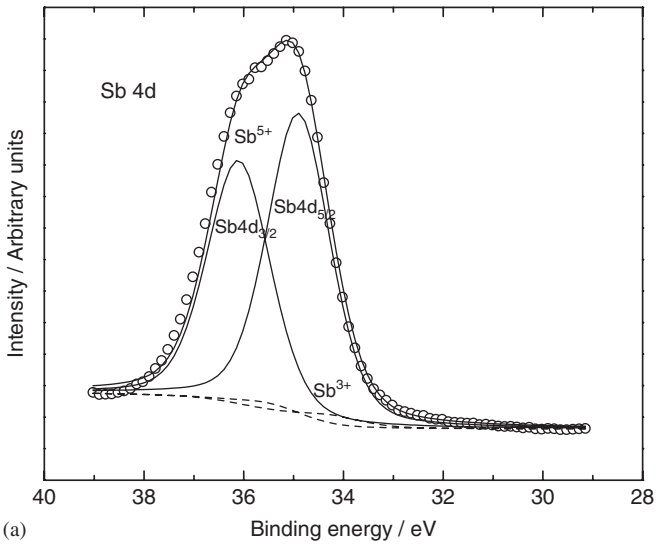


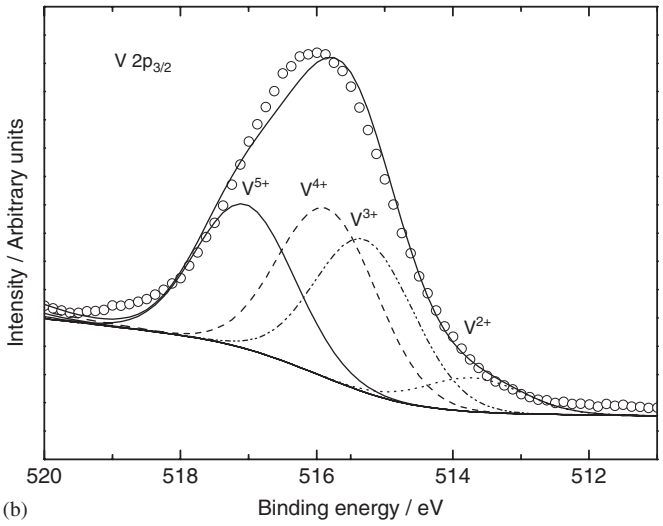


Fig. 4. Sb 4*d* and V 2*p* XPS spectra for the $VSbO_4$ sample after 0.5 min of argon sputtering.

in size, consistent with the crystal size value calculated from the XRD pattern. The $^{121}Sb$ Mossbauer spectrum, Fig. 3, exhibited a single-peak typical of $Sb^{5+}$. A $VSbO_4$ stochiometry was thus confirmed from the combination of XRD and Mossbauer data. The small absorption signal observed at $-12$ mm/s can be ascribed to the presence of $Sb^{3+}$ species. The calculated content was ca. 3% and probably came from un-reacted $Sb_2O_3$ remaining after milling. The XPS spectra confirmed these results. Fig. 4a shows the Sb 4*d* spectrum—the strongest peak for this element, 3*d*, and, particularly, the component $3d_{5/2}$, could no be analyzed because its binding energy is coincident with that of O 1*s* peak—was fitted to two components the binding energies (BE) of which are listed in Table 1. The higher BE was assigned to $Sb^{5+}$ and the lower one to $Sb^{3+}$ [23] the minor component. The V 2*p* spectrum, Fig. 4b, was more complex and fitted to four chemical environments ($V^{5+}$, $V^{4+}$, $V^{3+}$ and $V^{2+}$, in decreasing order of binding energy). The first three peaks had a similar contribution and accounted for more than 90% of the overall spectrum. The presence of V in high valence states is consistent with the strong reducing power of $V^{3+}$ and its oxidation in contact with air. This can explain why part of $V^{3+}$ was oxidized to a mixture of $V^{4+}$ and $V^{5+}$ at the surface level. In any case, these results show that grinding is an effective method for preparing highly pure $VSbO_4$ in nanometric particle size.

The reactivity of the compound towards Li was initially monitored by step potential electrochemical spectroscopy (SPES). Fig. 5 shows the SPES curves for Li/$VSbO_4$ cells as obtained in different potential ranges. The first cathodic curve for $VSbO_4$ recorded between 3.7 and 0.0 V, Fig. 5a, exhibited two broad, strong peaks at 1.35 and 0.75 plus an unresolved peak below 0.3 V. As expected, the discharge profile for this curve, Fig. 5b, exhibited two extended plateaux at ca. 1.3 and 0.7 V responsible for the previous peaks. The Li amount inserted at the end of the latter plateau was about 11.5 atoms per mole of compound, which is somewhat greater than that consumed in the following reactions:

$$VSbO_4 + 8\ Li \rightarrow Sb + V + 4\ Li_2O, \quad (1)$$

$$Sb + 3\ Li \rightarrow Li_3Sb. \quad (2)$$

Table 1
Binding energies (eV) for the Sb $4d_{5/2}$ photoemission peak in $VSbO_4$ sample before and after the electrochemical process

| Sample | $Ar^+$ sputtering time/min | Antimony valence state | | | |
|---|---|---|---|---|---|
| | | $-x$ | 0 | +3 | +5 |
| $VSbO_4$ | 0.5 | — | — | 34.2 (3) | 34.9 (97) |
| $VSbO_4$ electrode discharged at 0.5 V | 16 | 31.2 (26) | 32.5 (56) | 34.4 (18) | — |
| $VSbO_4$ electrode charged at 2.0 V | 4 | — | 32.5 (76) | 34.5 (24) | — |

Values in brackets are the atomic percentages.

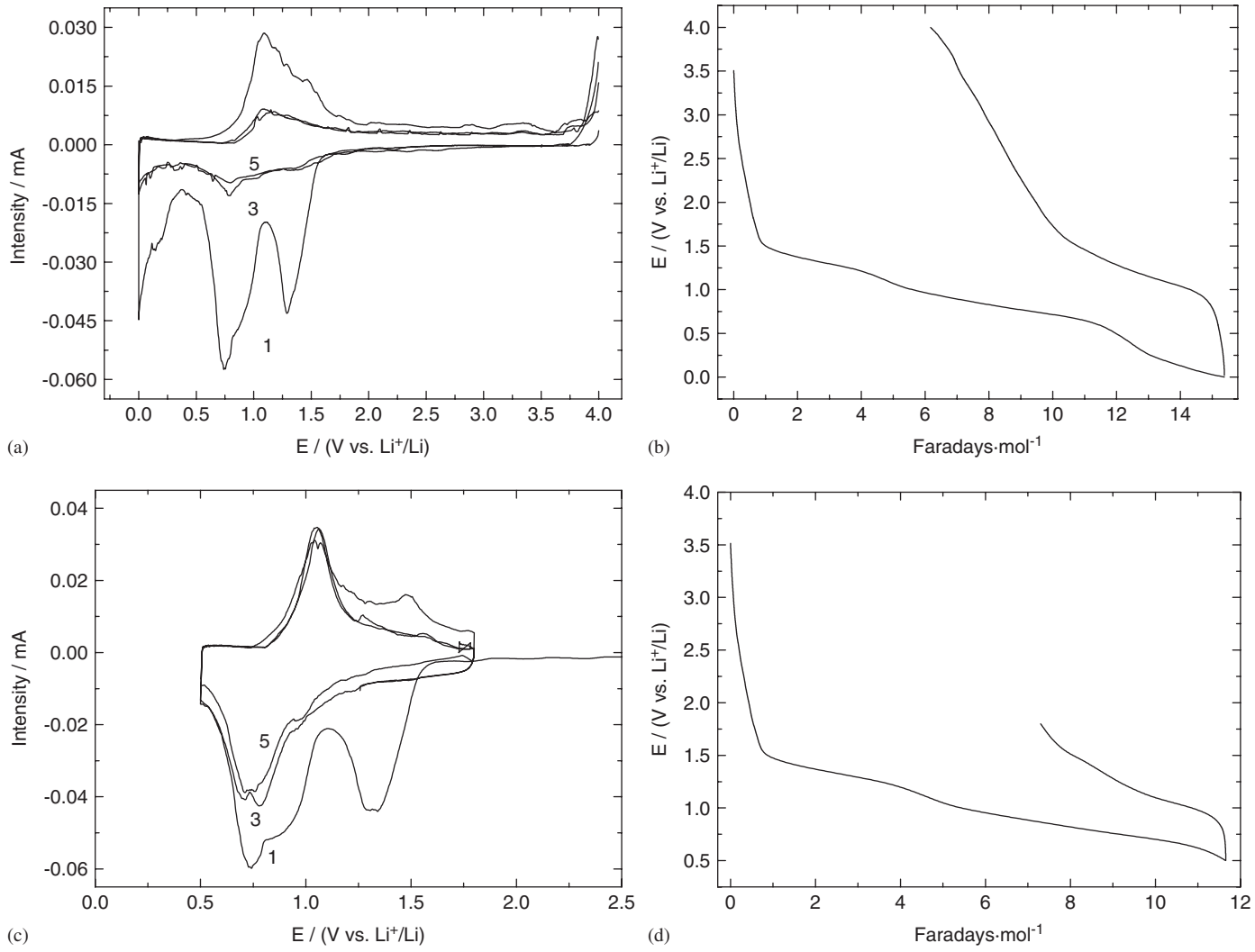


Fig. 5. Step potential curves (a, c) for the first, third and fifth cycle of the Li/$VSbO_4$ cell as recorded in different potential windows. (b, d) Potential vs. capacity plot corresponding to SPES curves (a) and (c), respectively.

The shape of the SPES curve is quite similar to that reported for the electrochemical reaction of other based Sb compounds such as $Sb_2O_3$ and $SbPO_4$ [18–20] with Li, which also exhibit two peaks of which that appearing at the higher voltage is ascribed to the formation of Sb particles according to

$$Sb_2O_3 + 6\,Li \rightarrow 2\,Sb + 3\,Li_2O \quad (3)$$

and that observed at the lower to the formation of Li–Sb alloys of composition $Li_2Sb$ or $Li_3Sb$ [2–9,18–20]. In our case, the asymmetry of both peaks might reflect a multistep mechanism for reactions (1) and (2) due to the presence of V and the formation of $Li_2Sb$ as an intermediate species, respectively. The additional capacity observed below 0.3 V can be ascribed to partial electrolyte decomposition catalysed by metallic particles forming a solid electrochemical interface (SEI) film [24].

Charging the cell to 4 V produced a broad asymmetric peak at 0.7–1.75 V that might correspond to the reverse process for the reduction peak observed at 0.7 V (viz. the de-alloying of $Li_3Sb$). Identifying a peak associated with the reverse reaction defined by Eq. (1) proved more difficult. In fact, the potential vs. de-inserted Li plot (Fig. 5b) exhibited a single plateau above 1 V, followed by continuous polarization up to 4 V. The amount of Li removed, around 9 Li atoms per mole of compound, suggests that reaction (1) is somewhat reversible. However, the following cycles resulted in a pronounced decrease in the intensity of the peaks in both the cathodic and anodic scans (Fig. 5a); this suggests that reactions (1) and (2) are irreversible in this voltage window. The formation of an SEI film of significant thickness as a consequence of the electrolyte decomposition might reduce the mobility of the charge carriers and decrease the rates of reactions (1) and (2) as a result. This was further confirmed by modifying the potential window to 1.8–0.5 V. Under these conditions, the step associated to the electrolyte decomposition and its polarization—the origin of which is unclear—was suppressed. The corresponding SPES curves, Fig. 5c, exhibit the main characteristics of the curves of Fig. 5a, but are consistent with the reversibility in reaction (2) on cycling (the calculated capacity, 4 Li atoms per mole of compound, Fig. 5d, was somewhat higher than that predicted from the reaction) and limited reversibility in reaction (1) as revealed by the low intensity of the high-voltage peak in the anodic scan, which gradually vanished with cycling.

The exact role played by V is unclear. In fact, there is some controversy concerning the ability of vanadium compounds to act as negative electrodes in Li batteries. According to Denis et al. [25], orthorhombic $InVO_4$ can react reversibly with up to 7 Li atoms per mole of compound, whereas $CrVO_4$ reacts irreversibly with Li. Other compounds such as $MnV_2O_6$ [26] also react reversibly with Li. In all these compounds, the vanadium is formally as $V^{5+}$. In our compound, $V^{3+}$ must be the main oxidation state; also, from the above described electrochemical results, it can hardly react reversibly with Li.

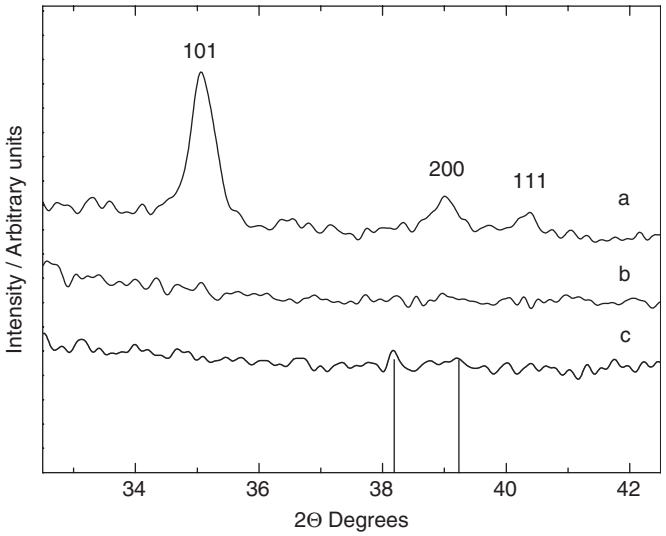


Fig. 6. XRD patterns for $VSbO_4$ electrode discharged at (a) 1.5 V, (b) 1.0 V and (c) 0.5 V. [–: $Li_3Sb$ pattern].

The structural and electronic changes undergone by $VSbO_4$ upon reaction with Li were examined from ex situ XRD patterns and XPS measurements. Fig. 6 shows the XRD patterns for the compound at three different discharge depths (1.5, 1.0 and 0.5 V). At 1.5 V, where the Faradaic yield was 0.5 Li per $VSbO_4$ mole, the XRD pattern was similar to that for the pristine sample (Fig. 1). The system retained its tetragonal structure, with a slight expansion (0.17 $Å^3$) of the unit cell volume. The low signal-to-noise ratio observed in the XRD patterns for the sample discharged at 1.0 and 0.5 V (Fig. 5a) precluded the identification of crystalline phases. This is indicative of drastic amorphization of the compound upon Li insertion and, unfortunately, prevents the identification of the products suggested for reactions (1) and (2). This is also a common occurrence in other Sb-based systems such as $SbPO_4$ [20].

The ex situ XPS measurements of the discharged and charged electrode were affected by the presence of electrolyte impurities on the electrode surface, even though it was washed carefully with acetonitrile. This impurity layer decreased the intensity of the photoemission peaks for the active material, thus concealing the electronic changes that occurred during the electrochemical process. In order to remove the electrolyte impurities, the electrode was sputtered with argon over short periods. Because the instability of the low oxidation states of V precluded obtaining information about the electronic changes in this element, the discussion will focus on Sb. Fig. 7a shows the Sb 4*d* spectrum for the electrode discharged up to 0.5 V and cleaned for 4 min. Based on Fig. 5, all Sb should be alloyed with Li and V in metallic form at this discharge depth. Compared with the spectrum of the original sample, Fig. 4, a shoulder is observed in the low BE region that can be assigned to the F 2*s* photoemission peak and ascribed to $LiPF_6$ traces adsorbed on the electrode surface. This peak tended to disappear as the sputtering time (Fig. 7b) was

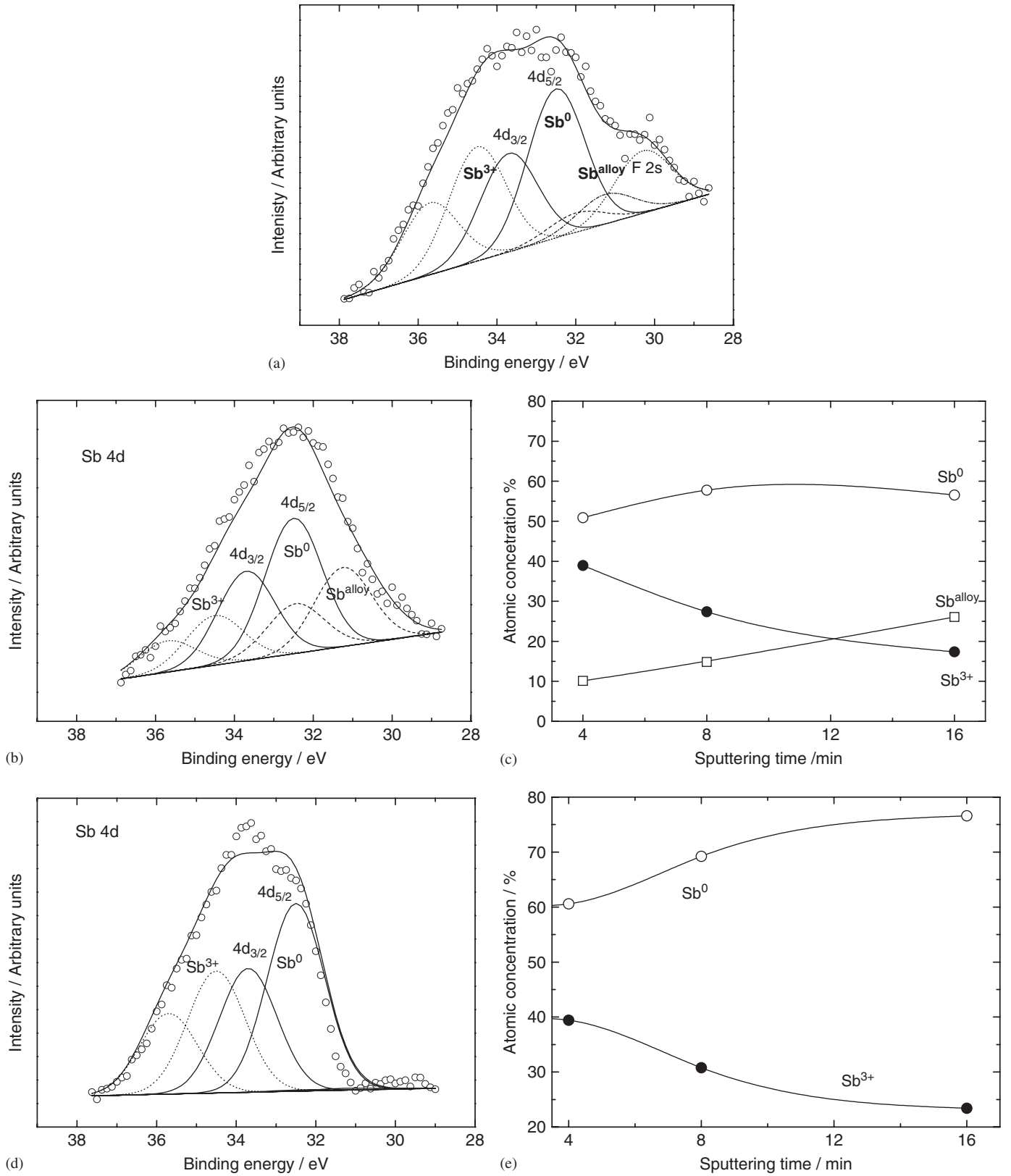


Fig. 7. Sb 4*d* XPS spectra for $VSbO_4$. (a, b) Electrode discharged at 0.5 V, and sputtered for 4 and 16 min, respectively. (d) Electrode charged at 2.0 V and sputtered for 4 min. (c, e) Atomic percentages for the different antimony valence states as a function of sputtering the time for the discharged and charged electrode, respectively.

increased. The best fit for this latter spectrum was obtained with three components for the Sb signal the BE of which are listed in Table 1. The two higher BE components are consistent with oxidized Sb ($Sb^{3+}$). The peak at 32.5 eV can be assigned to $Sb^0$ and the lowest energy peak at 31.2 to the element bound to Li in the $Li_xSb$ alloy. Sb in a chemical environment alloyed to Li has not been reported in the literature previously. The depth profile of this electrode is shown in Fig. 7c as the variation of the concentration of the three Sb species as a function of the sputtering time. The main observation is an increase in alloyed Sb content and a decrease in those of the other three species (particularly the oxidized species $Sb^{3+}$, the origin of which could be contact with oxygen traces). The origin of the high $Sb^0$ content is unclear. An oxidation process such as that proposed for the presence of $Sb^{3+}$ is unlikely as its content changed little with the sputtering time. A conversion of alloyed Sb to elemental Sb caused by either the X-ray beam and/or $Ar^+$ bombardment cannot be excluded but requires confirmation. In fact, the interconversion of the Sb oxidation states upon $Ar^+$ bombardment has recently been suggested [27].

Fig. 7d shows the Sb 4*d* spectrum obtained after charging the cell at 2.0 V. The main difference from the discharged electrode was the weakness of the F 2*s* peak, which suggests lower impurity content in this electrode. Moreover, only two Sb chemical environments were required to fit the profile. Their BE, listed in Table 1, are consistent with $Sb^0$ and $Sb^{3+}$. The predominant species was $Sb^0$. Its concentration increased with increasing bombardment time, Fig. 7e, and reached nearly 80% of the total Sb content after 16 min. The absence of the low-energy peak and the presence of $Sb^0$ as the main component is consistent with the model of electrochemical reactivity towards Li derived from the SPES curve, namely: the reversibility of reaction (2) and the difficulty of oxidizing the Sb formed after the de-alloying process.

The cycling properties of the cells made from $VSbO_4$ were examined from galvanostatic measurements, a more usual regime for analyzing this cell parameter. Based on the above considerations, two voltage windows were selected (viz. 2.5–0.5 and 1.5–0.5 V). Fig. 8 shows the variation of the discharge capacity as a function of the cycle number. The initial capacities for the wide and narrow window (650 and 450 A h/kg, respectively) markedly exceed that calculated from Eq. (2) (339 A h/kg). However, the delivered capacity faded with cycling in both cells, especially in the wider voltage range—possibly as a result of the increased polarization observed in the charge curve above 1.5 V, Fig. 6. Thus, although increasing the voltage window the delivered capacity increased, both cells delivered a similar capacity (around 250 A h/kg) in the 30th cycle. As noted earlier, the beneficial effect of V on cell performance is arguable if one also consider the difficulty of directly comparing our results with those reported for other Sb-based compounds (viz. $Sb_2O_5$ [19], $Sb_2O_3$ [18], Sb alloys [2–11]) as a consequence of the different conditions used (particle size, electrode preparation, voltage window, charge/discharge rate). Nevertheless, the electrochemical properties of $VSbO_4$ are better than those of $SbPO_4$ [20], a closely related compound. The formation of metal V in the first discharge process against $Li_3PO_4$, a poor electronic conductor, could explain the improved cell performance obtained by replacing P with V.

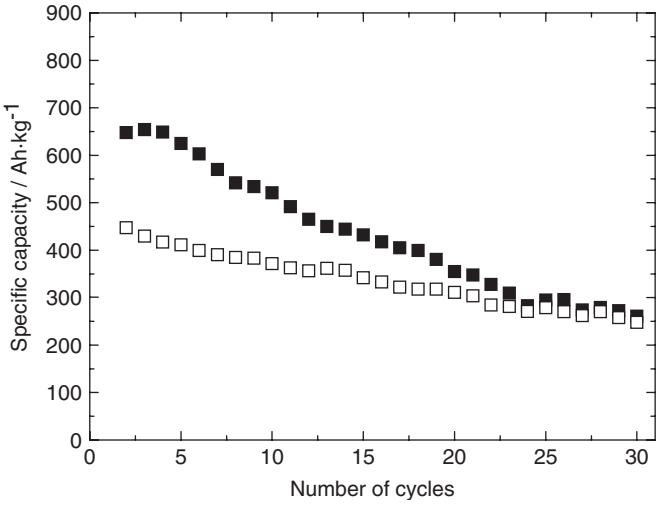


Fig. 8. Specific discharge capacity of the $Li/VSbO_4$ cell as a function of the number of cycles. Potential windows: (■) 2.5–0.5 V; (□) 1.5–0.5 V.

## 4. Conclusions

Nanosized $VSbO_4$ obtained by grinding a stoichiometric mixture of the respective oxides has the ability to react reversibly with Li at a low potential vs. the Li electrode and is a potential candidate to act as anode in a Li battery. The galvanostatic and SPES curves obtained for the $Li/VSbO_4$ cell were interpreted by assuming two reactions, namely: (i) complete, irreversible reduction of V and Sb over the 3.7–1.1 V range; and (ii) formation of $Li_nSb$ alloys at lower potentials. The latter reaction is reversible, but reversibility is reduced by the formation of an SEI film at discharge depths up to 0.0 V.

The reaction with Li completely destroyed the rutile-like framework and precluded identification of the resulting phases by X-ray diffraction. This difficulty was overcome by using the XPS technique, which exposed the electronic changes undergone by $VSbO_4$ upon reaction with Li. Fitting the Sb 4*d* peak of the electrode discharged at 0.0 V exposed a low energy component at 31.2 eV consistent with a chemical environment for Sb other than $Sb^0$ or $Sb^{n+}$. This component, ascribed to alloyed Sb, disappeared on charging the cell at 2.0 V. Under these conditions, $Sb^0$ was the main species found. All these results are consistent with a reversible alloying/de-alloying reaction, $Sb + nLi \Leftrightarrow Li_nSb$ ($n = 2, 3$), and confirm the difficulty of oxidizing the Sb once formed during the discharge process.

The capacity delivered by the $Li/VSbO_4$ cell as measured in the voltage windows 2.5–0.5 and 1.5–0.5 V faded on cycling—more markedly in the broader window—and

levelled of at around 250 A h/kg, a value somewhat lower than that estimated from reaction (2), 339 A h/kg—after 30 cycles. However, the capacity was higher than that for $SbPO_4$, which is isostoichiometric with the V compound. The formation of V as an inert metallic matrix countering the insulating properties of $Li_3PO_4$ could be the origin of the improved capacity delivered by the cell.

## Acknowledgments

This work was funded by Junta de Andalucía (Group FQM-175) and Spain's Ministry of Science and Technology (Project MAT2002-04477-C02-02). Professor Luis Sánchez also wishes to acknowledge award of a Journal Grant (03 07 451) by The Royal Society of Chemistry.

## References

[1] Y. Idota, M. Mishima, M. Miyaki, T. Kubota, T. Misayaka, Eur. Pat. Appl. 651450 (A1) (1997) 950503.
[2] D. Larcher, L.Y. Beaulieu, O. Mao, A.E. George, J.R. Dahn, J. Electrochem. Soc. 147 (2000) 1703.
[3] L.M.L. Fransson, J.T. Vaughey, K. Edström, M.M. Thackeray, J. Electrochem. Soc. 150 (2003) A86.
[4] J. Xie, X.B. Zhao, G.S. Cao, M.J. Zhao, Y.D. Zhong, L.Z. Deng, Mater. Lett. 57 (2003) 4673.
[5] L.J. Zhang, X.B. Zhao, X.B. Jiang, C.P. Lu, G.S. Cao, J. Power Sources 94 (2001) 92.
[6] X.B. Zhao, G.S. Cao, C.P. Lv, L.J. Zhang, S.H. Hu, T.J. Zhu, B.C. Zhou, J. Alloys Compd. 315 (2001) 265.
[7] J. Xie, G.S. Cao, X.B. Zhao, Y.D. Zhong, M.J. Zhao, J. Electrochem. Soc. 151 (2004) A1905.
[8] J. Xie, X.B. Zhao, G.S. Cao, M.J. Zhao, S.F. Su, J. Alloys Compd. 393 (2005) 283.
[9] S.-W. Song, R.P. Reade, E.J. Cairns, J.T. Vaughey, M.M. Thackeray, K.A. Striebel, J. Electrochem. Soc. 151 (2004) A1012.
[10] K.C. Hewitt, L.Y. Beaulieu, J.R. Dahn, J. Electrochem. Soc. 148 (2001) A402.
[11] M. Winter, J.O. Besenhard, Electrochim. Acta 45 (1999) 31.
[12] L.M.L. Fransson, J.T. Vaughey, R. Benedek, K. Edström, J.O. Thomas, M.M. Thackeray, Electrochem. Commun. 3 (2001) 317.
[13] V. Pralong, J.B. Leriche, B. Beaudoin, E. Naudim, M. Morcrette, J.M. Tarascon, Solid State Ionics 166 (2004) 295.
[14] J. Xie, X.B. Zhao, G.S. Cao, S.F. Su, J. Electrochem. Soc. 152 (2005) A601.
[15] I.A. Courtney, J.R. Dahn, J. Electrochem. Soc. 144 (1997) 2045.
[16] M. Martos, J. Morales, L. Sánchez, Electrochim. Acta 46 (2000) 83.
[17] N. Sharma, K.M. Shaju, G.V. Rao, B.V.R. Chowdari, Electrochem. Commun. 4 (2002) 947.
[18] H. Li, X. Huang, L. Chen, Solid State Ionics 123 (1999) 189.
[19] J. Santos, J. Cuart, I. Sandu, D.M. Schleich, T. Brousse, new trends in intercalation compounds for energy storage conversion, in: C. Julien, K. Zaghib (Ed.), The Electrochemical Society Proceedings Series, Pennington, NJ, 2003.
[20] J. Santos, J. Cuart, A. Caballero, J. Morales, L. Sánchez, J. Solid State Chem. 177 (2004) 2920.
[21] F.J. Berry, X. Ren, J. Mater. Sci. 39 (2004) 1179.
[22] H.P. Klug, L.E. Alexander, X-ray Diffraction Procedures for Polycrystalline and Amorphous Materials, Wiley, New York, 1974, p. 665.
[23] J.F. Moulder, N.F. Stickle, P.E. Sobol, K.D. Bomben, in: J. Chastain (Ed.), Handbook of X-ray Photoelectron Spectroscopy, PHI, Eden Prairie, 1995 (p. 129).
[24] J. Li, H. Li, Z. Wang, L. Chen, X. Huang, J. Power Sources 107 (2002) 1.
[25] S. Denis, E. Baudrin, F. Orsini, G. Ouvrard, M. Touboul, J.M. Tarascon, J. Power Sources 81–82 (1999) 79.
[26] S.-S. Kim, H. Ikuta, M. Wakihara, Solid State Ionics 139 (2001) 57.
[27] R. Reiche, J.P. Holgado, F. Yubero, J.P. Espinos, A.R. González-Elipe, Surf. Interface Anal. 35 (2003) 256.